Behavioral, Parameterized, and Broadband Modeling of Wired Interconnects with Internal Discontinuities

Contents lists available at ScienceDirect

Computer Methods and Programs in Biomedicine

journal homepage: www.elsevier.com

Automated detection and classification of liver fibrosis stages using contourlet transform and nonlinear features

U Rajendra Acharya[a, b, g], U Raghavendra[c], Joel E W Koh[a], Kristen M Meiburger[e, *], Edward J Ciaccio[d], Yuki Hagiwara[a], Filippo Molinari[e], LeongWai Ling[f], Anushya Vijayananthan[f], Nur Adura Yaakup[f], Mohd Kamil Bin Mohd Fabell[f], YeongChai Hong[f, g]

[a] *Department of Electronics and Computer Engineering, Ngee Ann Polytechnic, Clementi 599489, Singapore*
[b] *Department of Biomedical Engineering, School of Science and Technology, Singapore University of Social Sciences, Clementi 599491, Singapore*
[c] *Department of Instrumentation and Control Engineering, Manipal Institute of Technology, Manipal Academy of Higher Education, Manipal 576104, India*
[d] *Department of Medicine, Columbia University, USA*
[e] *Department of Electronics and Telecommunications, Politecnico di Torino, Corso Duca degli Abruzzi, 24, 10129 Torino, Italy*
[f] *Department of Biomedical Imaging, Faculty of Medicine, University of Malaya, 50603 Kuala Lumpur, Malaysia*
[g] *School of Medicine, Faculty of Health and Medical Sciences, Taylor's University, 47500 Subang Jaya, Malaysia*

ARTICLE INFO

Article history:
Received 17 April 2018
Received in revised form 24 August 2018
Accepted 1 October 2018
Available online xxx

Keywords:
Computer-aided diagnosis
Liver fibrosis
Contourlet transform
Texture features
Probabilistic neural network

ABSTRACT

Background and objective

Liver fibrosis is a type of chronic liver injury that is characterized by an excessive deposition of extracellular matrix protein. Early detection of liver fibrosis may prevent further growth toward liver cirrhosis and hepatocellular carcinoma. In the past, the only method to assess liver fibrosis was through biopsy, but this examination is invasive, expensive, prone to sampling errors, and may cause complications such as bleeding. Ultrasound-based elastography is a promising tool to measure tissue elasticity in real time; however, this technology requires an upgrade of the ultrasound system and software. In this study, a novel computer-aided diagnosis tool is proposed to automatically detect and classify the various stages of liver fibrosis based upon conventional B-mode ultrasound images.

Methods

The proposed method uses a 2D contourlet transform and a set of texture features that are efficiently extracted from the transformed image. Then, the combination of a kernel discriminant analysis (KDA)-based feature reduction technique and analysis of variance (ANOVA)-based feature ranking technique was used, and the images were then classified into various stages of liver fibrosis.

Results

Our 2D contourlet transform and texture feature analysis approach achieved a 91.46% accuracy using only *four* features input to the probabilistic neural network classifier, to classify the five stages of liver fibrosis. It also achieved a 92.16% sensitivity and 88.92% specificity for the same model. The evaluation was done on a database of 762 ultrasound images belonging to five different stages of liver fibrosis.

Conclusions

The findings suggest that the proposed method can be useful to automatically detect and classify liver fibrosis, which would greatly assist clinicians in making an accurate diagnosis.

1. Introduction

Chronic liver diseases are common and have become a major global health issue [1]. The degree of liver fibrosis has been identified as one of the most important diagnostic and prognostic assessments in chronic liver diseases [2]. Liver fibrosis is caused by unrelenting deposition of collagen fibers, due to the activation of hepatic stellate cells [2,3]. If liver fibrosis is left untreated, it may lead to cirrhosis and hepatocellular carcinoma. Liver transplantation is the only curative treatment for end-stage cirrhosis, but unfortunately it can only be done in a minority of patients due to the limited number of organs available [1]. Data from the Global Burden of Disease Study 2015 [4] showed that liver cirrhosis is one of the leading causes of death worldwide. Therefore, it is important to diagnose and treat liver fibrosis as early as possible, before it progresses to liver cirrhosis.

There are several scoring systems used for liver fibrosis assessment. The METAVIR system, commonly used for scoring, classifies liver fibrosis into *five* stages F0: no fibrosis, F1: minimal fibrosis (portal fibrosis without septa), F2: moderate or clinically sig-

* Corresponding author.
Email address: kristen.meiburger@polito.it (K.M. Meiburger)

https://doi.org/10.1016/j.cmpb.2018.10.006
0169-2607/

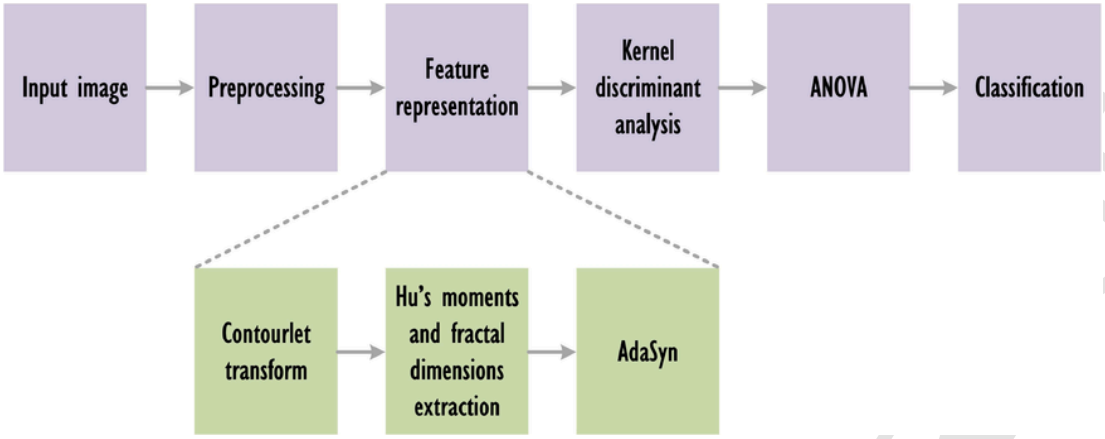

Fig. 1. Schematic diagram of the proposed technique.

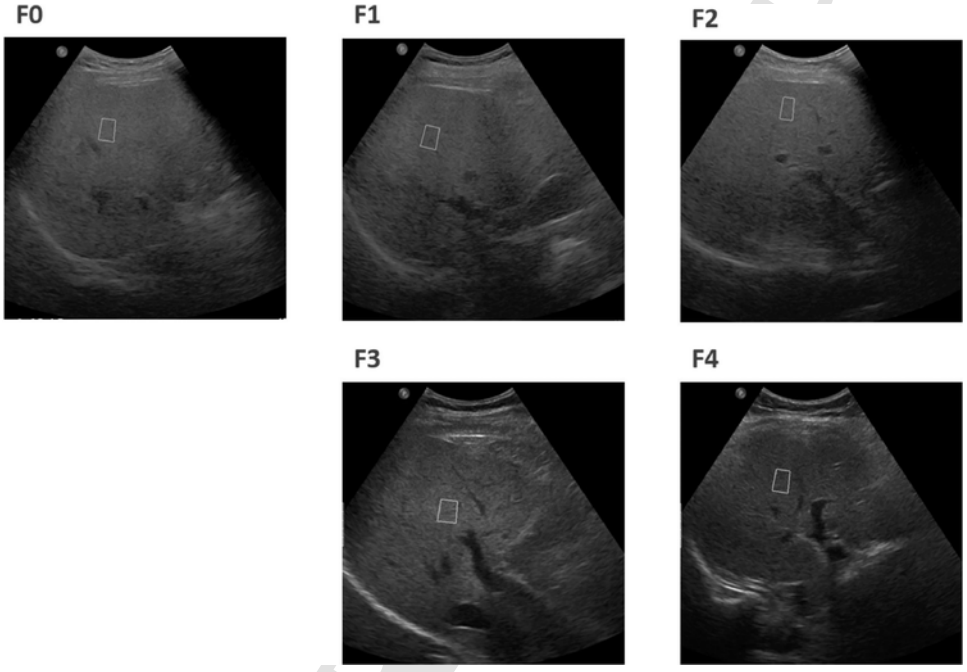

Fig. 2. Sample ultrasound images belonging to different liver fibrosis stages. F0: no fibrosis, F1: minimal fibrosis, F2: moderate or clinically significant fibrosis, F3: severe fibrosis, F4: cirrhosis.

nificant fibrosis (portal fibrosis with a few septa), F3: severe fibrosis (septal fibrosis with many septa but no cirrhosis), F4: cirrhosis.

Previously, the only available method to assess liver activity and fibrosis was liver biopsy. However the examination is invasive, prone to sampling errors, expensive, and associated with a significant risk of complications, such as hemorrhage, puncture of viscus, inadvertent biopsy of the kidney or the pancreas, and intrahepatic arteriovenous fistula formation [5]. In the past decade, liver biopsy has been gradually replaced by non-invasive techniques, such as transient elastography (TE), magnetic resonance elastography (MRE) and ultrasound elastography (USE) [6–9].

Several image processing techniques have been introduced for ultrasound imaging of liver diseases. The four traditional methods are described as follows. Ogawa et al. [10] proposed an artificial neural network for classifying diffuse liver disease into seven image features. For a database of 20 images, they achieved a maximum of 90% sensitivity using a neural network classifier. Wu et al. [11] introduced a multi-resolution fractal feature method based on the fractional Brownian motion model for characterizing three classes of ultrasonic liver images (normal, hepatoma and cirrhosis). They used 90 images belonging to three different groups and achieved a 90% classification rate using a Bayes classifier. Mojsilović et al. [12] described a new approach that utilized energies of the transformed regions of the image based on wavelet decomposition. For the database of 244 liver images, the overall accuracy was 90%. Yeh et al. [13] employed image features extracted from the gray level co-occurrence matrix and wavelet decomposition, which were later tested by the support vector machine (SVM) classifier. They incorporated 100 images belonging to six different stages of liver disease and achieved a maximum 91% accuracy for normal and abnormal classification. Recently, Khvostikov et al. [14] have shown the advantage of anisotropic diffusion for liver fibrosis diagnosis. A total of 140 regions of interest (ROIs) were evaluated in their study and achieved a maximum performance of 90% classification accuracy. The

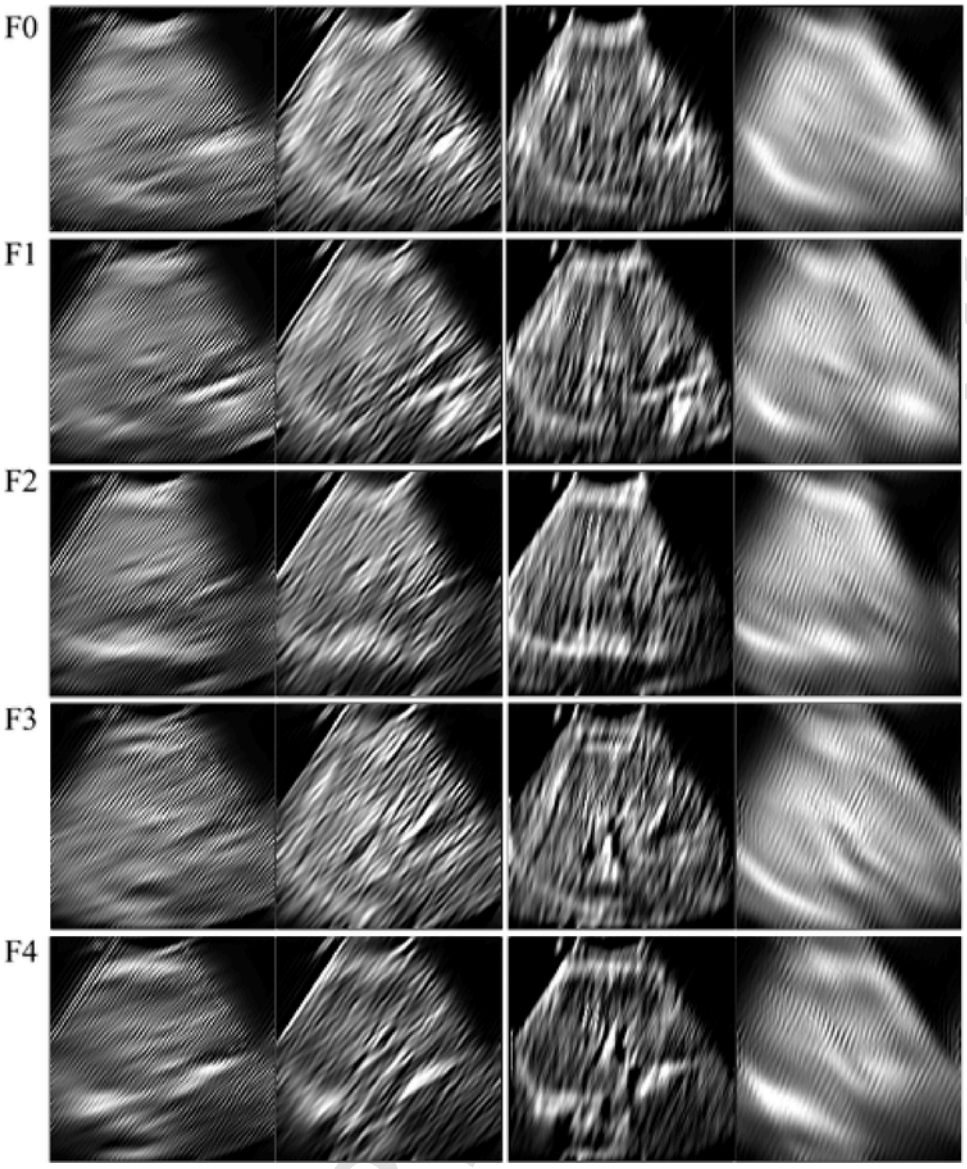

Fig. 3. First level contourlet coefficients of fibrosis stages (from left to right: first, second, third and fourth coefficient). F0–F4: the five stages of liver fibrosis.

Table 1
Number of samples before and after applying AdaSyn.

Stages	No. of samples before AdaSyn	No. of samples after AdaSyn
F0	164	325
F1	304	304
F2	48	299
F3	206	268
F4	40	303

above-mentioned techniques, however, have several disadvantages, including a limited number of extracted features, the setting of features based on subjective human experience, and the inability to dynamically optimize the techniques when changes are made to the dataset. These limitations may be overcome by using deep learning techniques. Many computer aided diagnosis (CAD) systems were developed to detect liver disease using ultrasound images [15–20]. Various researchers have used deep learning for CAD, using both clinical data and liver ultrasound images [21–24].

Table 2
Performance of different feature reduction techniques using ANOVA feature ranking.

Data reduction method	Classifier	No of features	$F_{acc.}$ (%)	F_{PPV} (%)	$F_{sen.}$ (%)	$F_{spe.}$ (%)
PCA	PNN	24	83.59	97.06	81.52	91.08
MFA	PNN	8	78.19	94.81	76.32	84.92
LSDA	PNN	25	90.79	99.15	89.01	97.23
LPP	SVM Poly3	26	77.59	96.15	74.36	89.23
KPCA (poly plus)	SVM RBF	20	78.12	94.15	76.83	82.77
KPCA (polynomial)	SVM RBF	20	78.12	94.15	76.83	82.77
KDA (poly plus)	PNN	4	91.46	96.78	92.16	88.92
KDA (polynomial)	PNN	4	91.46	96.78	92.16	88.92

*$F_{acc.}$: Accuracy, F_{sen}: Sensitivity, $F_{spe.}$: Specificity.

Table 3
Performance of different feature ranking techniques using KDA feature reduction.

Feature selection method	Classifier	No of features	$F_{acc.}$ (%)	F_{PPV} (%)	$F_{sen.}$ (%)	$F_{spe.}$ (%)
ACO	PNN	10	80.05	93.88	79.73	81.23
ANOVA	PNN	4	91.46	96.78	92.16	88.92
GA	PNN	10	79.12	93.53	78.79	80.31
PSO	PNN	10	81.12	94.68	80.41	83.69
ACO-GA	PNN	10	77.12	92.88	76.66	78.77
SFS-*k*-NN	PNN	10	71.98	89.52	72.74	69.23

*$F_{acc.}$ Accuracy, $F_{sen.}$: Sensitivity, $F_{spe.}$: specificity.

From the literature review, a limited number of works have addressed fibrosis classification. Although a few researchers attempted to resolve this problem, many of them utilized a limited dataset of ultrasound images during evaluation. In addition, evaluation for all stages of liver fibrosis remains an open problem for investigators. This paper proposes a novel algorithm using the contourlet transform, coupled with nonlinear features, to automatically classify the *five* stages of liver fibrosis with 762 ultrasound images collected from 236 patients.

The extracted feature dimensions are reduced using different techniques and are then selected and ranked using conventional techniques. The final refined features are incorporated into a classifier for validation.

2. Material and methods

Fig. 1 shows the schematic diagram of our proposed technique. The details of each processing stage are described in the subsequent sections.

2.1. Data collection

In order to validate our proposed liver fibrosis classification technique, we have collected a total of 762 ultrasound images from 236 patients (120 males, 116 females, aged 55.4 ± 9.7 years old) belonging to five different classes of liver fibrosis. Three to four images were obtained from each patient. The images were acquired prospectively at the University of Malaya Medical Centre, Kuala Lumpur, Malaysia using an ultrasound system (Epiq 7G, Philips, Massachusetts, United States). Medical ethics approval was obtained from

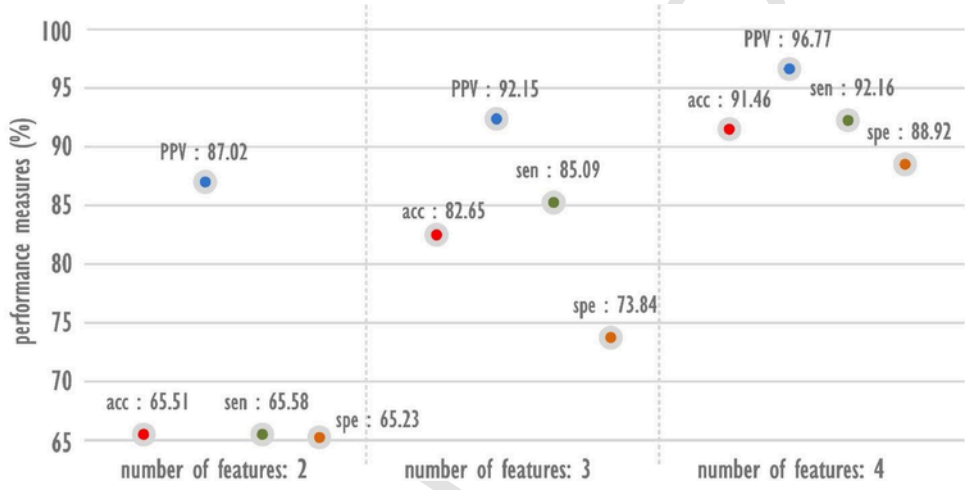

Fig. 4. Different performance parameters for various number of features.

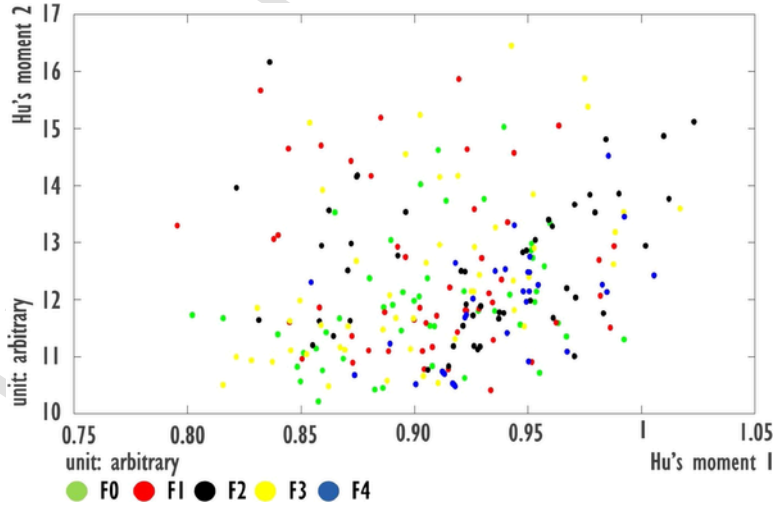

Fig. 5. Scatter plot of Hu's moment features.

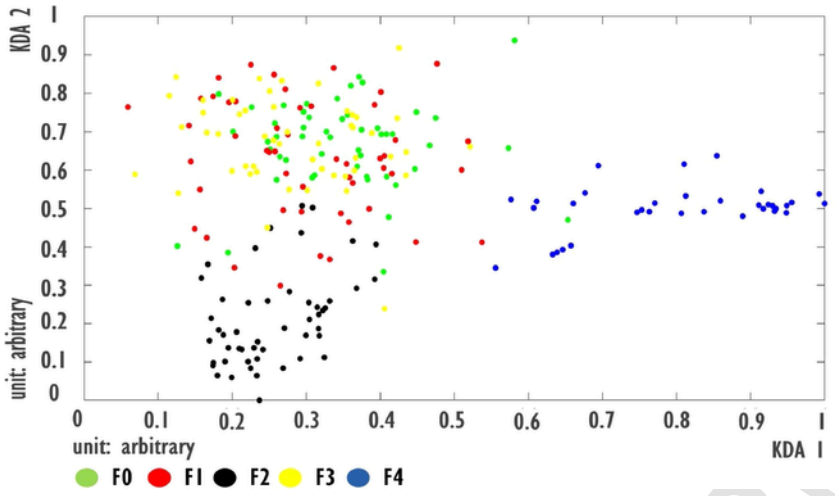

Fig. 6. Scatter plot of KDA features.

the Institutional Ethics Committee (Medical Ethics Approval No. MECID 20170103-4332). Written informed consent was obtained from all of the patients recruited in this study. The stage of liver fibrosis was confirmed by biopsy. Ultrasound imaging was done using a convex probe (C5-1 convex Probe, Philips, Massachusetts, United States) with ultrasound frequency = 3.5 MHz, image depth = 15 cm, dynamic range = 70 dB, with image size = 1384 × 2026 pixels. Fig. 2 shows examples of ultrasound images belonging to different fibrosis stages.

2.2. Data pre-processing

All of the images were initially pre-processed using contrast limited adaptive histogram equalization (CLAHE) [25]. This process enhanced the visibility level of the image by adaptively improving the contrast of a local region, termed a tile. Thereafter, all neighboring tiles were stitched seamlessly, using interpolation, to obtain the final enhanced image.

2.3. Feature representation

The proposed feature representation involves three processing stages: (1) contourlet transform, (2) feature extraction and (3) synthetic sample generation. The details of each stage are described in the following paragraphs.

2.3.1. Contourlet transform

The contourlet transform is a 2D transform method for image representation, which shows a more dispersed and better approximation performance when compared to other multiscale analysis tools [26–30]. Its primary roles are multiscale and multidimensional decomposition. The contourlet transform can efficiently capture the contours of original images, which are the discriminative features, with few coefficients.

It includes double filter bank construction to obtain the smooth curves of images. Initially, a Laplacian filter (LP) is employed to detect discontinuities, and a directional filter bank (DFB) constructs discontinuity points into linear structures [26,31,32]. DFB is suitable for high frequency and exhibits directionality in its sub bands. It leads to 2^i sub bands, where i is the level of decomposition. In this work, similar filters are used for LP and DFB, as given in [28,33–35]. Decomposition is performed up to the third level, which results in *sixteen* coefficients. These decomposition levels are empirically fixed based upon repeated experiments, which renders maximum performance. Fig. 3 shows the sample coefficients of first level decomposition. These coefficients are used for extracting features in the next section.

2.3.2. Feature extraction

In our method, we have extracted numerous features from the contourlet transformed coefficients, namely Hu's moments, log energy, Fourier energy and fractal dimensions.

Hu's moments: Hu's moments are a useful representation technique that summarize invariant image patterns. The two-dimensional Hu's image moments $f(x, y)$ can be defined as:

$$m_{pq} = \sum_x \sum_y x^p y^q f(x,y) \tag{1}$$

For nonnegative values of p and q, the central moments can be defined as:

$$\mu_{pq} = \sum_x \sum_y (x-\bar{x})^p (y-\bar{y})^q f(x,y) \tag{2}$$

$$where\ \bar{x} = \frac{m_{10}}{m_{00}}\ \ and\ \ \bar{y} = \frac{m_{01}}{m_{00}}$$

are the image centroid. Hence, the normalized central moments of the above equation are given by:

$$\begin{aligned}\delta_{pq} &= \frac{\mu_{pq}}{\mu_{00}^{\tau}}, for p, q \\ &= 0, 1, 2, 3, \ldots, where\ \tau \\ &= \frac{p+q}{2} + 1\end{aligned}$$

From the above normalized moments, *seven* different Hu moments as denoted in [34] are extracted. They are invariant to scale and orientation, and effectively represent the invariant patterns of an image. The invariant moments are:

$$HM1 = \delta_{20} + \delta_{02} \tag{3}$$

$$HM2 = \left(\delta_{20} - \delta_{02}\right)^2 + 4\delta_{11}^2 \tag{4}$$

$$HM3 = \left(\delta_{30} - 3\delta_{12}\right)^2 + \left(3\delta_{21} - \delta_{03}\right)^2 \tag{5}$$

$$HM4 = \left(\delta_{30} + \delta_{12}\right)^2 + \left(\delta_{21} + \delta_{03}\right)^2 \tag{6}$$

$$HM5 = \left(\delta_{30} - 3\delta_{12}\right)\left(\delta_{30} + \delta_{12}\right)\left[\left(\delta_{30} + 3\delta_{12}\right)^2 - 3\left(\delta_{21} + \left(3\delta_{21} - \delta_{03}\right)\left(\delta_{21} + \delta_{03}\right)\left[3\left(\delta_{30} + \delta_{12}\right)^2 - \left(\delta_{21} + \delta_{03}\right)^2\right]\right.\right.$$

$$HM6 = \left(\delta_{20} - \delta_{02}\right)\left[\left(\delta_{30} + \delta_{12}\right)^2 - \left(\delta_{21} + \delta_{03}\right)\right] + 4\delta_{11}\left(\delta_{30} + \delta_{12}\right)\left(\delta_{21} + \delta_{03}\right)$$

$$HM7 = \left(3\delta_{21} - \delta_{03}\right)\left(\delta_{30} + \delta_{12}\right)\left[\left(\delta_{30} + \delta_{12}\right)^2 - 3\left(\delta_{21} + \delta_{03}\right)^2\right] + \left(3\delta_{12} - \delta_{30}\right)\left(\delta_{21} + \delta_{03}\right)\left[3\left(\delta_{30} + \delta_{12}\right)^2 - \left(\delta_{21} + \delta_{\ldots}\right)\right.$$

Fractal dimensions (FD): FD describes another invariant representation of an image, preserving invariant shape even if there is significant shrinking or magnification of image objects. It also represents irregular and roughness of pixel intensities. In this work, we have used the differential box counting method of FD computation as given in [36,37]. In addition to FD, Fourier energy and log energy features are also computed from the contourlet coefficients. In total, *ten* features are extracted using the Hu's moments and FD techniques.

2.3.3. Synthetic samples generation

Imbalanced data samples generally introduce bias toward majority classes. Synthetic sample generation is a technique that generates synthetic data to the minority class by understanding the topological structure of the majority classes. In this work, we have used the adaptive synthetic sampling (AdaSyn) technique to balance the samples in the minority and majority classes [38]. AdaSyn involves both minority and majority classes during processing and adds additional synthetic samples to the minority class. In this study, F_1 has a maximum number of samples as compared to the other classes. We have generated synthetic samples based upon the generated features which are listed in Table 1. The table shows the details of samples belonging to liver fibrosis stages before and after implementation of AdaSyn.

2.4. Feature dimensionality reduction

Feature reduction techniques are useful to reduce the dimensionality of an original features set. These techniques compute compactness and separability of intra class and inter class, respectively, so as to maintain a large separation between inter class data samples. In addition, a greater number of projections will be created, which assists in clustering intra class data points. In this work, we have used Locality Sensitive Discriminant Analysis (LSDA) [39], Marginal Fisher Analysis (MFA) [40], Principal Component Analysis (PCA) [41], Kernel Principal Component Analysis (KPCA) [42] (kernels: polyplus and polynomial), Locality Preserving Projections (LPP) [43], and Kernel Discriminant Analysis (KDA) (kernels: polyplus and polynomial) [44–46].

2.5. Optimal feature selection

Feature selection techniques are an essential tool that is required for machine learning. They work by finding an optimal paradigm to select a subset of features that can boost the overall performance of any algorithm. In this work, we have used a set of conventional feature selection techniques, such as Analysis of Variance (ANOVA) [47], Ant Colony Optimization (ACO) [48], genetic algorithm (GA) [49], and Particle Swarm Optimization (PSO) [50, 51], for selecting the most significant features. We have also used a combination of ACO-GA [52] and Sequential Forward Selection (SFS) – *k*-nearest neighbor (*k*-NN) [53,54] techniques.

2.6. Feature classification

Classification techniques are the predictive methods that determine the true class of the test labels. Supervised algorithms are the most powerful technique in this category, and initially partition the input data into training and testing sets, then train the network using different parameters. During testing, class labels of the test samples are identified. In this work, we have used *k*-nearest neighbor (*k*-NN) [53], Decision Tree (DT) [54], Linear Discriminant Analysis (LDA) [55], Quadratic Discriminant Analysis (QDA) [55], Probabilistic Neural Network classifier (PNN) [56], and SVM (with kernels: polynomial of Orders 1–3) [57] to test the feature set. Different statistical performance metrics, namely sensitivity, specificity, accuracy, and positive predicted value (PPV), are computed in order to evaluate the developed technique. A ten-fold based cross-validation scheme is used in order to remove bias toward training and testing features. The algorithm was developed in MATLAB with a *Core i5* processor (RAM: 4 GB).

3. Experimental results

The ultrasound images of *five* different liver fibrosis stages were initially pre-processed using CLAHE and then subjected to the contourlet transform. The transformed images were used to generate *sixteen* feature maps. In total, *ten* features were extracted from each feature map, which resulted in *one hundred and sixty* features. The obtained features were subjected to AdaSyn for synthetic samples generation. AdaSyn synthetically created additional samples for minority classes and the details are given in Table 1. Further, these features were subjected to different feature dimensionality reduction techniques. Reduced features were then fed to different feature selection algorithms for the selection of optimal features. Finally, the significant features were fed to different classifiers to test the developed model. Tables 2 and 3 present the obtained best performances. The proposed model achieved a maximum performance of 91.46% accuracy, 92.16% sensitivity, and 88.92% specificity for the KDA data reduction technique with ANOVA feature ranking. A satisfactory performance was also achieved using the LSDA data reduction tech-

nique with ANOVA ranking; however, this method required 25 features, which extends the computation time. Fig. 4 presents the performance of ANOVA for a different number of features. Fig. 5 shows the scatter plot of the original Hu's moment features. Fig. 6 shows the class separability of KDA1 and KDA2 features. It can also be observed that the data samples from different classes are more clustered using KDA in Fig. 6 as compared with Fig. 5.

4. Discussion

The mortality and incidence rate of liver cirrhosis have recently increased [1–3]. This growth can be controlled by timely personalized treatment. In this work, we have proposed an efficient technique for classification of liver fibrosis stages using the contourlet transform and invariant texture features. The contourlet feature transform has several important properties, namely multiresolution, directionality, and anisotropy, which can efficiently represent uniqueness among various stages over different multiresolution levels [26–28]. It results in different visual representations among various stages of liver fibrosis, as shown in Figs. 2 and 3. Also, textural features have highlighted invariant shapes in each stage, which is assistive to discriminate abnormalities [36, 37, 58]. AdaSyn has generated more robust synthetic samples which have addressed the complexity issue related to class imbalance among different stages of fibrosis. The proposed method has achieved a maximum performance of 91.46% accuracy for only *four* features using KDA, ANOVA and PNN classifiers (Please Ref. Tables 2 and 3). In order to test the robustness of our method, we have compared various feature reduction and also ranking techniques. It is observed that our proposed method outperformed all of the other techniques, in terms of the number of features required, and also in terms of performance parameters. It is observed that the KDA projected features are more efficient and separable as compared with the original Hu's moment features. It is to be noted that our method is the first attempt in classifying the five different stages of liver fibrosis with a maximum performance. These extracted KDA features are further classified using PNN classifier to yield highest classification performance. But, the specificity of our developed system is comparatively less than the accuracy, PPV and sensitivity. This may be because few KDA features belonging to the normal class have been classified as other fibrosis classes.

The developed multiresolution approach requires minimum features to attain maximum performance compared to other feature reduction and ranking techniques. The PNN classifier has performed the best among all other techniques. It also required a minimum feature set in all other experiments (Please Ref. Tables 2 and 3). In the future, we plan to enhance the performance by recruiting a larger number of subjects and also plan to use deep learning techniques [59,60].

The uniqueness of our method are the use of a multiresolution analysis and textural features for liver fibrosis classification. We have analyzed 762 ultrasound images with KDA feature reduction and ANOVA feature ranking. We have achieved a highest performance of 91.46% accuracy using only *four* significant textural features.

5. Conclusions

In this study, a fully automated system to classify the severity of liver fibrosis stages using the contourlet transform and nonlinear features is developed. The developed method can be useful to grade the severity of input ultrasound images among *five* different stages of liver fibrosis. A maximum performance of 91.46% accuracy was achieved using a PNN classifier. The performance of our developed prototype requires additional validation on a larger database. Hence, in the future, we plan to include an increased pool of subjects in each of the *five* different stages, to improve method performance. Such a system can be potentially beneficial to radiologists to confirm diagnosis. Also, we will extend the developed model using deep learning architectures.

Conflict of interest

The authors declare no conflict of interest.

References

[1] P. Ginès, I. Graupera, F. Lammert, P. Angeli, L. Caballeria, A. Krag, I.N. Guha, S.D. Murad, L. Castera, Screening for liver fibrosis in the general population: a call for action, Lancet Gastroenterol. Hepatol. 1 (3) (2016) 256–260.

[2] R.A. Standish, E. Cholongitas, A. Dhillon, A.K. Burroughs, A.P. Dhillon, An appraisal of the histopathological assessment of liver fibrosis, Gut 55 (4) (2006) 569–578.

[3] C.Y. Zhang, W.G. Yuan, P. He, J.H. Lei, C.X. Wang, Liver fibrosis and hepatic stellate cells: etiology, pathological hallmarks and therapeutic targets, World J. Gastroenterol. 22 (48) (2016) 10512.

[4] H. Wang, M. Naghavi, C. Allen, R.M. Barber, A. Carter, D.C. Casey, F.J. Charlson, A.Z. Chen, M.M. Coates, M. Coggeshall, L. Dandona, Global, regional, and national life expectancy, all-cause mortality, and cause-specific mortality for 249 causes of death, 1980–2015: a systematic analysis for the global burden of disease study 2015, The Lancet 388 (10053) (2016) 1459–1544.

[5] F.M. Sanai, E.B. Keeffe, Liver biopsy for histological assessment – the case against, Saudi J. Gastroenterol. 16 (2) (2010) 124.

[6] J.L. Gennisson, T. Deffieux, M. Fink, M. Tanter, Ultrasound elastography: principles and techniques, Diagn. Interv. Imaging 94 (5) (2013) 487–495.

[7] G. Ferraioli, C. Tinelli, B. Dal Bello, M. Zicchetti, R. Lissandrin, G. Filice, C. Filice, E. Above, G. Barbarini, E. Brunetti, W. Calderon, M. Di Gregorio, R. Gulminetti, P. Lanzarini, S. Ludovisi, L. Maiocchi, A. Malfitano, G. Michelone, L. Minoli, M. Mondelli, S. Novati, S.F. Patruno, A. Perretti, G. Poma, P. Sacchi, D. Zanaboni, M. Zaramella, Performance of liver stiffness measurements by transient elastography in chronic hepatitis, World J. Gastroenterol. 19 (2013) 49–56.

[8] J.E. Lee, J.M. Lee, K.B. Lee, J.H. Yoon, C.I. Shin, J.K. Han, B.I. Choi, Noninvasive assessment of hepatic fibrosis in patients with chronic hepatitis B viral infection using magnetic resonance elastography, Korean J. Radiol. 15 (2014) 210–217.

[9] G. Ferraioli, P. Parekh, A.B. Levitov, C. Filice, Shear wave elastography for evaluation of liver fibrosis, J. Ultrasound Med. 33 (2014) 197–203.

[10] K. Ogawa, M. Fukushima, K. Kubota, N. Hisa, Computer-aided diagnostic system for diffuse liver diseases with ultrasonography by neural networks, IEEE Trans. Nuclear Sci. 45 (6) (1998) 3069–3074.

[11] C.M. Wu, Y.C. Chen, K.S. Hsieh, Texture features for classification of ultrasonic liver images, IEEE Trans. Med. Imaging 11 (1992) 141–152.

[12] M.P. Mojsilovic, S. Markovic, M. Krstic, Characterization of visually similar diffuse diseases from B-scan liver images using nonseparable wavelet transform, IEEE Trans. Med. Imaging 17 (4) (1998) 541–549.

[13] W. Yeh, S. Huang, P. Li, Liver fibrosis grade classification with B-mode ultrasound, Ultrasound Med. Biol. 29 (9) (2003) 1229–1235.

[14] A. Khvostikov, A. Krylov, J. Kamalov, A. Megroyan, Ultrasound despeckling by anisotropic diffusion and total variation methods for liver fibrosis diagnostics, Signal Process. Image Commun. 59 (2017) 3–11.

[15] U.R. Acharya, U. Raghavendra, H. Fujita, Y. Hagiwara, J.E.W. Koh, J.H. Tan, V.K. Sudarshan, A. Vijayananthan, C.H. Yeong, A. Gudigar, K.H. Ng, Automated characterization of fatty liver disease and cirrhosis using curvelet transform and entropy features extracted from ultrasound images, Comput. Biol. Med. 79 (2016) 250–258.

[16] U.R. Acharya, J.E.W. Koh, Y. Hagiwara, J.H. Tan, A. Gertych, A. Vijayananthan, N.A. Yaakup, B.J.J. Abdullah, M.K.B.M. Fabell, C.H. Yeong, Automated diagnosis of focal liver lesions using bidirectional empirical mode decomposition features, Comput. Biol. Med. 94 (2018) pp.11–pp.18.

[17] U.R. Acharya, S.V. Sree, R. Ribeiro, G. Krishnamurthi, R.T. Marinho, J. Sanches, J.S. Suri, Data mining framework for fatty liver disease classification in ultrasound: a hybrid feature extraction paradigm, Med. Phys. 39 (7) (2012) 4255–4264.

[18] U.R. Acharya, O. Faust, F. Molinari, S.V. Sree, S.P. Junnarkar, V.K. Sudarshan, Ultrasound-based tissue characterization and classification of fatty liver disease: a screening and diagnostic paradigm, Knowl.-Based Syst. 75 (2015) 66–77.

[19] U.R. Acharya, H. Fujita, V.K. Sudarshan, M.R.K. Mookiah, J.E.W. Koh, J.H. Tan, Y. Hagiwara, K.C. Chua, S.P. Junnarkar, A. Vijayananthan, K.H. Ng, An integrated index for identification of fatty liver disease using radon transform and discrete cosine transform features in ultrasound images, Inf. Fusion 31 (2016) 43–54.
[20] U.R. Acharya, H. Fujita, S. Bhat, U. Raghavendra, A. Gudigar, F. Molinari, A. Vijayananthan, K.H. Ng, Decision support system for fatty liver disease using GIST descriptors extracted from ultrasound images, Inf. Fusion 29 (2016) 32–39.
[21] R. Miotto, L. Li, B.A. Kidd, J.T. Dudley, Deep patient: An unsupervised representation to predict the future of patients from the electronic health records, Sci. Rep. 6 (2016) 26094.
[22] P. Nguyen, T. Tran, N. Wickramasinghe, S. Venkatesh, DeepR: a convolutional net for medical records, IEEE J. Biomed. Health Inf. 21 (1) (2017) 22–30.
[23] L. Nie, M. Wang, L. Zhang, S. Yan, B. Zhang, T.S. Chua, Disease inference from health-related questions via sparse deep learning, IEEE Trans. Knowl. Data Eng. 27 (8) (2015) 2107–2119.
[24] D. Meng, L. Zhang, G. Cao, W. Cao, G. Zhang, B. Hu, Liver fibrosis classification based on transfer learning and FCNet for ultrasound images, IEEE Access 5 (2017) 5804–5810.
[25] S.M. Pizer, E.P. Amburn, J.D. Austin, R. Cromartie, A. Geselowitz, T. Greer, B.T.H. Romeny, J.B. Ximmerman, K. Zuiderveld, Adaptive histogram equalization and its variations, Comput. Vis. Graph. Image Process. 39 (3) (1987) 355–368.
[26] P. Amorim, T. Moraes, D. Fazanaro, J. Silva, H. Pedrini, Electroencephalogram signal classification based on shearlet and contourlet transforms, Exp. Syst. Appl. 67 (2017) 140–147.
[27] D.D.Y. Po, M.N. Do, Directional multiscale modeling of images using the contourlet transform, IEEE Trans. Image Process. 15 (6) (2006) 1610–1620.
[28] S. Zhang, G. Yang, Z. Cheng, H.V.D. Wetering, C. Ikuta, Y. Nishio, A novel optimization design approach for contourlet directional filter banks, Inst. Electron. Inf. Commun. Eng. Electron Exp. 11 (17) (2014) 1–11.
[29] A. Rouhafzay, N. Baaziz, M. Diop, Contourlet versus Gabor transform for texture feature extraction and image retrieval, In: 2016.
[30] S. Katsigiannis, E.G. Keramidas, D. Maroulis, Contourlet transform for texture representation of ultrasound thyroid images, in: H. Papadopoulos, A.S. Andreou, M. Bramer (Eds.), Artificial Intelligence Applications and Innovations", IFIP Advances in Information and Communication Technology, 339, Springer, Berlin, Heidelberg, 2010.
[31] R.H. Bamberger, M.J.T. Smith, A filter bank for the directional decomposition of images: theory and design, IEEE Trans. Signal Process. 40 (4) (1992) 882–893.
[32] P. Burt, E. Adelson, The Laplacian pyramid as a compact image code, IEEE Trans. Commun. 31 (4) (1983) 532–540.
[33] U.R. Acharya, H. Fujita, V.K. Sudarshan, S.L. Oh, M. Adam, J.H. Tan, J.H. Koo, A. Jain, C.M. Lim, K.C. Chua, Automated characterization of coronary artery disease, myocardial infarction, and congestive heart failure using contourlet and shearlet transforms of electrocardiogram signal, Knowl.-Based Syst. 132 (2017) 156–166.
[34] A. Cohen, I. Daubechies, J.C. Feauveau, Biorthogonal bases of compactly supported wavelets, Commun. Pure Appl. Math. 45 (5) (1992) 485–560.
[35] S. Phoong, C.W. Kim, P.P. Vaidyanathan, R. Ansari, A new class of two-channel biorthogonal filter banks and wavelet bases, IEEE Trans. Signal Process. 43 (3) (1995) 649–665.
[36] M.K. Biswas, T. Ghose, S. Guha, P.K. Biswas, Fractal dimension estimation for texture images: a parallel approach, Pattern Recognit. Lett. 19 (3–4) (1998) 309–313.
[37] B.B. Mandelbrot, The Fractal Geometry of Nature, Freeman, San Francisco, 1982.
[38] H. He, B. Yang, E.A. Garcia, S.T. Li, ADASYN: adaptive synthetic sampling approach for imbalanced learning, In: Proceedings of the IEEE Transactional Joint Conference on Neural Networks, Hong Kong, China, 2008.
[39] D. Cai, X. He, K. Zhou, J. Han, H. Bao, Locality sensitive discriminant analysis, In: Proceedings of the Twentieth International Conference on Artificial Intelligence, Hyderabad, 2007.
[40] S. Yan, D. Xu, B. Zhang, Q. Yang, S. Lin, Graph embedding and extensions: a general framework for dimensionality reduction, IEEE Trans. Pattern Anal. Mach. Intell. 29 (1) (2007) 40–51.
[41] R.O. Duda, P.E. Hart, D.G. Stork, Pattern classification, second ed., John Wiley & Sons, New York, 2001.
[42] B. Scholkopf, A. Smola, K.R. Muller, Nonlinear component analysis as a kernel Eigenvalue problem, Neural Comput. 10 (5) (1998) 1299–1319.
[43] X. He, P. Niyogi, Locality Preserving Projections, University of Chicago, Chicago, 2004, Doctoral Dissertation.
[44] G. Baudat, F. Anouar, Generalized discriminant analysis using a kernel approach, Neural Comput. 12 (10) (2000) 2385–2404.
[45] D. Cai, Spectral Regression: A Regression Framework for Efficient Regularized Subspace Learning, University of Illinois, Urbana, Illinois, 2009, Doctoral Dissertation.
[46] D. Cai, X. He, J. Han, Speed up kernel discriminant analysis, Int. J. Very Large Data Bases 20 (1) (2011) 21–33.
[47] A. Gelman, Analysis of variance – why it is more important than ever, Ann. Stat. 33 (2005) 1–33.
[48] M. Dorigo, M. Birattari, T. Stutzle, Ant colony optimization, IEEE Comput. Intell. Mag. 1 (4) (2006) 28–39.
[49] M. Mitchell, "An Introduction to Genetic Algorithms", MA, USA: MIT Press, Cambridge, 1998.
[50] J. Kennedy, R. Eberhart, Particle swarm optimization, IEEE Int. Conf. Neural Netw. (1995).
[51] Y. Shi, R. Eberhart, A modified particle swarm optimizer, In: Proceedings of the IEEE World Congress on Computational Intelligence, Anchorage, AK, USA, 1998.
[52] S. Nemati, M.E. Basiri, N. Ghasem-Aghaee, M.H. Aghdam, A novel ACO–GA hybrid algorithm for feature selection in protein function prediction, Exp. Syst. Appl. 36 (10) (2009) 12086–12094.
[53] D.T. Larose, Discovering Knowledge in Data: An Introduction to Data Mining, John Wiley & Sons, 2005.
[54] D. Ververidis, C. Kotropoulos, Sequential forward feature selection with low computational cost, In: Proceedings of the Thirteenth European Signal Processing Conference, Antalya, Turkey, 2005.
[55] T.M. Cover, Geometrical and statistical properties of systems of linear inequalities with applications in pattern recognition, IEEE Trans. Electron. Comput. 14 (3) (1965) 326–334.
[56] D.F. Specht, Probabilistic neural networks, Neural Netw. 3 (1) (1990) 109–118.
[57] V. Kecman, Learning and Soft Computing: Support Vector Machines, Neural Networks, and Fuzzy Logic Models, MIT Press, MA, USACambridge, 2001.
[58] U. Raghavendra, N.S. Bhat, A. Gudigar, U.R. Acharya, Automated system for the detection of thoracolumbar fracture using a CNN architecture, Fut. Gen. Comput. Syst. 85 (2018) 184–189.
[59] M.K. Hu, Visual pattern recognition by moment invariants, IEEE Trans. Inf. Theory 8 (2) (1962) 179–187.
[60] U. Raghavendra, H. Fujita, S.V. Bhandary, A. Gudigar, J.H. Tan, U.R. Acharya, Deep convolution neural network for accurate diagnosis of glaucoma using digital fundus images, Inf. Sci. 441 (2018) 41–49.